The Journal of Experimental Biology 208, 2939-2949
Published by The Company of Biologists 2005
doi:10.1242/jeb.01733

Aquatic wing flapping at low Reynolds numbers: swimming kinematics of the Antarctic pteropod, *Clione antarctica*

Brendan J. Borrell[1,*], Jeremy A. Goldbogen[1] and Robert Dudley[1,2]

[1]*Department of Integrative Biology, University of California, Berkeley, CA 94720, USA* and [2]*Smithsonian Tropical Research Institute, P.O. Box 2072, Balboa, Republic of Panama*

*Author for correspondence (e-mail: bborrell@berkeley.edu)

Accepted 6 June 2005

Summary

We studied swimming kinematics of the Antarctic pteropod, *Clione antarctica*, to investigate how propulsive forces are generated by flexible oscillating appendages operating at low Reynolds numbers (10<*Re*<100). We filmed ten ascending individuals at 125 frames s^{-1} from two orthogonal views, and reconstructed three-dimensional coordinates of the wing tip and body. Each half-stroke of flapping consisted of distinct power and recovery phases, which were of approximately equal duration in both the upstroke and the downstroke. As pteropods ascended, the body traced a sawtooth path when viewed laterally. The magnitude of these oscillations decreased with body mass, and larger animals (operating at *Re*>25) exhibited gliding during the recovery phase of each half-stroke. Maximum translational and rotational accelerations of the body occurred at the initiation of each power phase, suggesting that rotational circulation, the acceleration reaction, and wake recapture may all potentially contribute to vertical force production. Individual contributions of these mechanisms cannot, however, be assessed from these kinematic data alone. During recovery phases of each half-stroke, *C. antarctica* minimized adverse drag forces by orienting the wings parallel to flow and by moving them along the body surface, possibly taking advantage of boundary layer effects. Vertical force production was altered through changes in the hydrodynamic angle of attack of the wing that augmented drag during the power phase of each half-stroke. At higher translational velocities of the body, the inclination of the power phase also became more nearly vertical. These results indicate that, in addition to serotonin-mediated modulation of wingbeat frequency reported previously in *Clione*, geometric alteration of wingbeat kinematics offers a precise means of controlling swimming forces.

Supplementary material available online at
http://jeb.biologists.org/cgi/content/full/208/15/2939/DC1

Key words: *Clione antarctica,* drag, flapping flight, kinematics, lift, pteropod, swimming.

Introduction

Flying and swimming animals across a range of sizes produce thrust by transferring momentum to the surrounding fluid medium using paired, oscillating appendages (Vogel, 1994). In general, propulsive forces are generated *via* two primary kinematic modes: flapping or rowing. In flapping locomotion, the propulsive appendages reciprocate in a stroke plane largely orthogonal to the resultant force vector. The lift force is the predominant component of force, and is directly proportional to the circulation of the vortex bound to the wing (Ellington, 1984c; Sane, 2003; Vogel, 1994). In rowing, propulsive forces are generated during the power stroke by both the drag force acting on a translating appendage in approximate proportion to the square of its instantaneous velocity, and by reaction forces generated by the acceleration of fluid relative to the body (Daniel, 1984; Vogel, 1994; Walker, 2002). The relative merits of flapping and rowing in different ecological and hydrodynamic contexts have been considered before, but researchers have yet to come to agreement on the relative efficiency of these two locomotor modes for small animals moving through either air or water (see Bellwood and Wainwright, 2001; Fish, 1996; Vogel, 1994; Walker, 2002; Walker and Westneat, 2000). One approach to the problem has been simply to catalog locomotor modes of organisms across a range of size scales, but this comparative approach has been hindered by a dearth of kinematic data on the smallest and slowest flapping animals, namely pteropods and flying insects (Walker, 2002).

A general problem for lift generation by such small organisms operating at lower Reynolds number (*Re*) is the rapid viscous dissipation of kinetic energy imparted to the surrounding fluid (Fuiman and Batty, 1997; Podolsky and Emlet, 1993; Vogel, 1994). Under such circumstances, the efficiency of flapping locomotion declines because bound

circulation decreases and viscous drag increases, resulting in impractical lift-to-drag ratios (Vogel, 1994). Rowing locomotion will also be hindered at low *Re* because fluid will fail to separate and translate away from oscillating appendages at the end of the power stroke. Consequently, drag during the power stroke may be only slightly greater than that during the recovery stroke (Walker, 2002). Furthermore, as the relative importance of inertial forces declines at low *Re*, reaction forces generated from unsteady motion of the rowing appendages will also diminish (Daniel, 1984; McHenry et al., 2003; Williams, 1994b).

In recognizing the effects of scale in biological fluid dynamics, researchers have often partitioned the dynamic spectrum into an inertial regime ($Re>1000$), a viscous regime ($Re<10$), and an intermediate regime ($1000>Re>10$; Daniel et al., 1992; Fuiman and Batty, 1997; Webb and Weihs, 1986). Fuiman and Batty (1997) manipulated the viscosity of water to show that fish larvae follow hydrodynamic predictions of the viscous regime up to $Re=300$, and also suggested that viscous effects could be significant even at *Re* as high as 450. Other studies of invertebrate larvae also supported the conclusion that inertial forces do not play a major role in propulsion at $Re<100$ (McHenry et al., 2003; Williams, 1994a,b). It is clear that we are coming closer to a mechanistic understanding of force generation at low to intermediate *Re*, and thus it is germane to explore stroke kinematics of organisms that may not fit established locomotor paradigms.

Clione antarctica, a pteropod mollusc found in Antarctic waters, is one of the smallest known aquatic flappers and uses its paired oscillating appendages known as pteropodia (henceforth, wings) to ascend in the pelagic water column. Morton (1954, 1958) suggested that thecosomatous (i.e. shelled) pteropods operating at about the same *Re* as *C. antarctica* use their wings strictly as paddles, producing thrust only once per stroke cycle, but also suggested that larger gymnosome (i.e. shell-less) pteropods such as *Clione limacina* produce thrust during both the upstroke and downstroke *via* a sculling motion. In a detailed kinematic study of pteropod locomotion, Satterlie et al. (1985) concluded that *C. limacina* produces thrust *via* lift forces and a clap-and-fling mechanism. However, the smaller size and lower wingbeat frequency of *C. antarctica*, when coupled with the higher viscosity associated with near-freezing polar waters, suggests that in spite of morphological and kinematic similarities with *C. limacina*, the underlying mechanisms of thrust production may differ. Thus, we examined wing stroke parameters and body kinematics of *C. antarctica* to develop a model for flapping force production in these diminutive swimmers. Our results suggest that *C. antarctica* modulates thrust in vertical ascent by altering the orientation of the power phase of each half-stroke, and that thrust at high velocities is generated primarily *via* steady-state drag, although rotational lift, the acceleration reaction and wake recapture (see Sane, 2003) may also be important.

Materials and methods

Study organism and filming

We conducted all experiments during December 2001 and January 2002 in the Crary Laboratory at McMurdo Station. During the austral summer, *Clione antarctica* Smith are abundant and easily collected from plankton tows through holes in the sea ice above the Ross Sea, or by using dip nets along rocky shores abutting the open waters of the sea. In late December, it was only possible to collect smaller pteropods (<5 mm), but as the season progressed we were able to collect individuals up to 20 mm in length. Ambient water temperature in McMurdo Sound is approximately –1.7°C. After capture, individuals were placed immediately in a cooler filled with seawater and transported to the laboratory, where they were acclimated and maintained in aquaria at temperatures near 0°C. For experimental studies, we selected only actively swimming individuals that had been maintained in captivity for no more than 4 days.

We constructed a filming chamber by lining a 500 ml finger bowl with a sheet of black plastic rolled into a truncated cone. This setup funneled pteropods into the field of view of the camera and also provided flapping individuals with adequate space during their ascent to avoid both physical contact with the substratum and potential boundary effects. A high-speed video camera (Redlake Imaging Motionscope, San Diego, CA, USA) was positioned approximately 1.5 m above the filming chamber to provide a frontal view of ascending animals. We ensured that the line of sight of the camera was orthogonal to the water surface (and largely parallel with the body axis of swimming individuals) by use of a spirit-level mounted on the camera. To simultaneously record frontal and lateral views of wingbeat kinematics, a front-surface mirror (40 mm×40 mm×56.5 mm) was placed in the filming chamber at 45° relative to the water's surface. Because of corrosion during the course of the study, later trials were filmed using a commercial-grade back-surface mirror. The width of these mirrors provided the spatial calibration for both frontal and lateral views. The experimental chamber was filled with filtered seawater obtained from McMurdo Sound, and the entire chamber was placed inside a variable-temperature water bath (Frigomix 1495; Braun Biotech International, Goettingen, Germany) filled with 50% propylene glycol to prevent freezing. Water bath temperature was monitored using a copper-constantan thermocouple (Barnant 100; Barrington, IL, USA) with a resolution of 0.1°C, placed on one side of the chamber, and/or a platinum thermometer placed on the opposite side of the chamber. We periodically stirred the seawater within the filming chamber and averaged temperature readings from each thermocouple/thermometer when both were available. Experimental water temperatures ranged from –1.8°C to 2.0°C.

Individual pteropods were placed within the filming chamber and allowed to acclimate for at least 10 min prior to filming. They were otherwise held at 0°C during each trial run. Two fiber optic microscope lamps illuminated the filming

chamber from above. Individuals ascended in the chamber of their own volition and, when doing so, were filmed at 125 frames s^{-1}. The relatively high framing rate of the video camera provided approximately 80 frames per wingbeat, corresponding to a high temporal resolution that was sufficient to determine the timing of kinematic events and to estimate the first and second derivatives of wing and body position.

Wingbeat geometry and body kinematics

To characterize representative kinematics, we selected ten ascent sequences in which the wings of the animal were clearly visible and the transverse body axis was orthogonal to the lateral filming view (i.e. <10° body roll relative to the mirror's edge). Using Quickimage, a modification of NIH Image distributed by J. Walker (www.usm.edu/~walker), the wing base and wingtip were digitized in both the lateral and frontal views. We measured wing length, R, as the maximum tip–base distance exhibited during a cycle. We also calculated the area of a wing pair, S, at midstroke by measuring the projected area in the top view and dividing it by the cosine of the wing angle with respect to the horizontal axis as measured simultaneously in the lateral view. This calculation of wing pair area was carried out for both the upstroke and the downstroke of each ascent sequence and was then averaged. From the wing angle at midstroke, we calculated the angle of attack, α, as the angle between the wing surface and β_{ps}, the stroke plane during the power phase of a half-stroke (see below for definition). The mean wing chord, $\bar{c}$, is the wing area divided by the span ($=S/2R$), and the aspect ratio (AR) equals $4R^2/S$. Stroke area is the area swept by the wing during a half-stroke and is related to the total force generated by an oscillating appendage.

Video sequences were then smoothed to reduce pixel noise and thresholded to provide a binary image from which the pteropod's image could be manually isolated from the background. The wings were then erased virtually from video images, and a geometric center of area of the body was determined for both the lateral and frontal views of the animal. Mean body velocity ($\hat{V}$) was expressed non-dimensionally as the number of wing lengths travelled per wingbeat. The angle between the horizontal x-axis and the mean path of ascent, ξ, was calculated using the mean body velocity vector in the y–z plane during the course of an entire wingbeat (see below). A second ascent angle, ξ_{ps} was calculated during the power phase only. Body angle (χ) was determined as the angle subtending the major axis of the animal and the vertical z-axis (Fig. 1). For each ascent sequence, we calculated a mean body angle, $\bar{\chi}$, and an angle of oscillation, χ_a, corresponding to the difference between the maximum and minimum values of χ during a single wingbeat.

Wingtip coordinates were transformed to a body-based coordinate system wherein the wing base corresponds to the origin, the z' axis is the anterior–posterior axis of the animal, and the x' axis corresponds to the line connecting the two wing bases (see Fig. 1). A linear regression of wingtip coordinates in the lateral view was used to calculate a mean stroke plane angle β between the flapping wings and the y' axis (see Walker and Westneat, 1997). The power stroke plane angle β_{ps} relative to the body was calculated from the mean wingtip velocity during the power stroke. As the wing translates through a wingstroke, its curvature changes continuously, with the wing being nearly straight during the middle of each half-stroke and maximally curved at the beginning and end of each half-stroke. Consequently, instead of transforming wingtip coordinates about the stroke plane and defining wingtip position in spherical coordinates (see Ellington, 1984b), we chose to present wingtip position in rectangular coordinates.

Finally, a spline function was fitted to the positional data derived from wingtip coordinates, body center of area and body angle. Velocity and acceleration estimates were then obtained using the program Quicksand (Walker, 1998). Time-standardized kinematics were produced from these functions by interpolating the ensuing estimates to 100 equally spaced points. These profiles were then aligned for eight ascent sequences based on the first minimum in the x position of the wing. We defined $\hat{t}$=0 as the initiation of the power phase of the upstroke, when the wing reaches a maximum in the z-axis. Averaging these profiles yielded mean positional data, velocity, and acceleration estimates for these eight sequences. Wingtip velocity in the transverse plane was calculated as the vector sum of velocity components in the (x', y') plane and an analogous calculation was made for fore–aft wingtip velocity in the sagittal plane (see Fig. 2A). Because steady-state lift and drag forces should be approximately proportional to the square of the transverse and fore–aft components of wingtip velocity, respectively, body accelerations would be predicted to coincide temporally with maximum wingtip velocities if unsteady mechanisms are unimportant. On the other hand, maximum body accelerations at the ends of half-strokes would strongly implicate such force-producing mechanisms as rotational circulation, wake capture and the acceleration reaction (see Sane, 2003).

Results

Over 400 sequences of *C. antarctica* ascending in the experimental chamber were obtained, and of these ten were selected that satisfied the following criteria for analysis: sequences represented at least one complete wingbeat, anterior and posterior tips of the body were visible during the full wingbeat cycle, and both wings and body were fully extended during the ascent (based on visual observation of the full set of experimental sequences). Additionally, the dorsoventral plane of the pteropod was nominally perpendicular to the lateral camera view in all analyzed sequences, and the wing nearest to the mirror was clearly visible in both lateral and top views (see Movies 1, 2 and 3 in supplementary material).

We calculated mean kinematic parameters from all ten sequences, but present wingtip positional data only for the eight sequences in which the digitized stroke was initiated on the ventral surface of the animal (i.e. the upstroke). Aspect ratio of the wings ranged from 1.66 to 4.47 (Table 1).

All data given subsequently are presented as the mean value ±1 S.E.M. (standard error of the mean).

Qualitative description of the wingbeat

A typical wingbeat of an ascending *C. antarctica* is presented in Fig. 1, together with vectors indicating instantaneous velocity and acceleration of the geometric center of body area. The wingbeat exhibits distinctive propulsive and recovery phases in each half-stroke, whereby ascent velocity during the each propulsive power phase exceeds ascent velocity during the recovery phase. As wing rotation begins at the end of the down- and upstrokes, wings are curved around the body with the wingtips nearly touching or overlapping (Fig. 1a,e). As the wings begin to straighten and translate posteriorly, they simultaneously twist along their length, initiating the power stroke (Fig. 1b,g). By mid-stroke, the wing has completely straightened out, and the wingtip has reached its maximum positional angle within the stroke (Fig. 1c,h). At this point in time, the body reaches its maximum translational velocity. Wings are distinctly cambered positively relative to the direction of wing motion. At the completion of the power phase of the half-stroke, the wings start to curl around the body (Fig. 1d,i). The wingtip then translates anteriorly along the body axis to recover for subsequent strokes (Fig. 1d–f).

When the body of the pteropod is viewed laterally, the path of the wingtip relative to the wing base resembles a distorted figure-of-eight that is wrapped around the anterior–posterior axis of the body (Fig. 2). The wingtip follows a counterclockwise path around the ventral loop of this figure-of-eight, and a clockwise path around the dorsal loop. Due to the slightly ventral location of the wing base, the wingtip path is not symmetrical about the body axis, and the paths traced out by the upstroke and downstroke intersect at a point approximately 10% of the wing length ventral to the wing base. For two individuals, we digitized two consecutive wingbeats, and observed no major differences in wing motion (see Fig. 2). Overall, the visual impression of wingbeat motions is one of very high repeatability among consecutive wingbeats during ascent.

Table 1. *Morphometric and hydrodynamic variables for ascending* Clione antarctica

Individual	L (mm)	R (mm)	AR	n (Hz)	Re_b	Re_w	J
1	7.12	2.41	2.68	1.58	18	32	0.14
2	8.40	2.57	4.47	1.47	6	15	0.06
3	9.99	2.91	2.21	1.51	33	48	0.18
4	10.24	2.30	1.81	1.39	33	51	0.16
5	10.85	2.63	2.16	1.62	22	51	0.10
6	11.11	3.05	2.56	1.49	37	53	0.15
7	11.15	3.82	2.79	1.42	15	64	0.06
8	14.12	4.07	2.77	1.22	49	64	0.16
9	19.83	4.73	1.63	0.81	36	107	0.10
10	21.54	4.49	1.66	1.14	43	123	0.09

L, body length; R, wing length; AR, aspect ratio; n, wingbeat frequency; Re_b, Reynolds number of the body; Re_w, Reynolds number of the wing; J, advance ratio.

Quantitative wingbeat kinematics

We define $\hat{t}$=0 as the beginning of the power phase of the upstroke, with the maximum wingtip velocity occurring between $\hat{t}$=0.08 and $\hat{t}$=0.14 (Fig. 3). The power phase ends at approximately $\hat{t}$=0.23. At $\hat{t}$=0.29, the wingtip typically rests against the dorsal surface of the animal and slowly moves anteriorly in preparation for the next half-stroke. At $\hat{t}$=0.36, the wing continues to move anteriorly, but spanwise curvature is progressively reduced. The wingtip reaches its most anterior point at $\hat{t}$=0.50, ending the half-stroke. The downstroke is largely symmetrical with respect to the upstroke. The mean wingbeat frequency, n, was 1.36±0.25 Hz. The ratio of the duration of the upstroke that of the downstroke, *US:DS*, averaged 0.98±0.05. Neither n nor the stroke area was significantly correlated with body translational velocity (P>0.1). The Re for the mean wing chord ranged from 15–123 (Table 1). However, Re of the mean wing chord during the power phase of the upstroke was nearly twice the mean value for the half-stroke, ranging from 26 to 223. The advance ratio J (calculated as the ratio of the mean ascent velocity to the

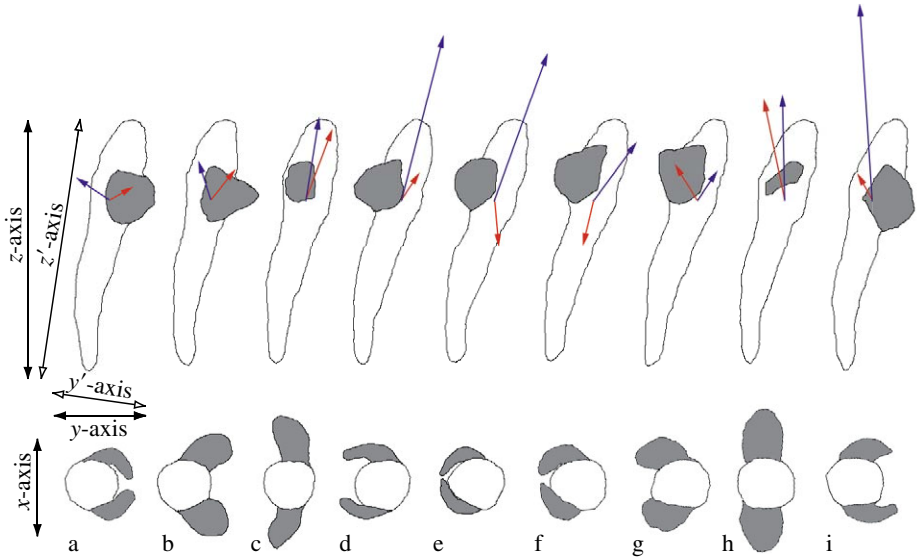

Fig. 1. Wingtip motion for a *Clione antarctica* during a single wingbeat cycle (a–i) from lateral (above) and dorsal (below) perspectives. Mean relative velocity of the body (blue arrows) and mean body acceleration vectors (red arrows) are averaged from data for eight individuals. The external coordinate system is shown indicating the x-, y- and z-axes. The body coordinate system is indicated by the y'- and z'-axes, but, in this example, the x'-axis is not shown because it is coincident with the x-axis. The origin of the body coordinate system is at the near wing base.

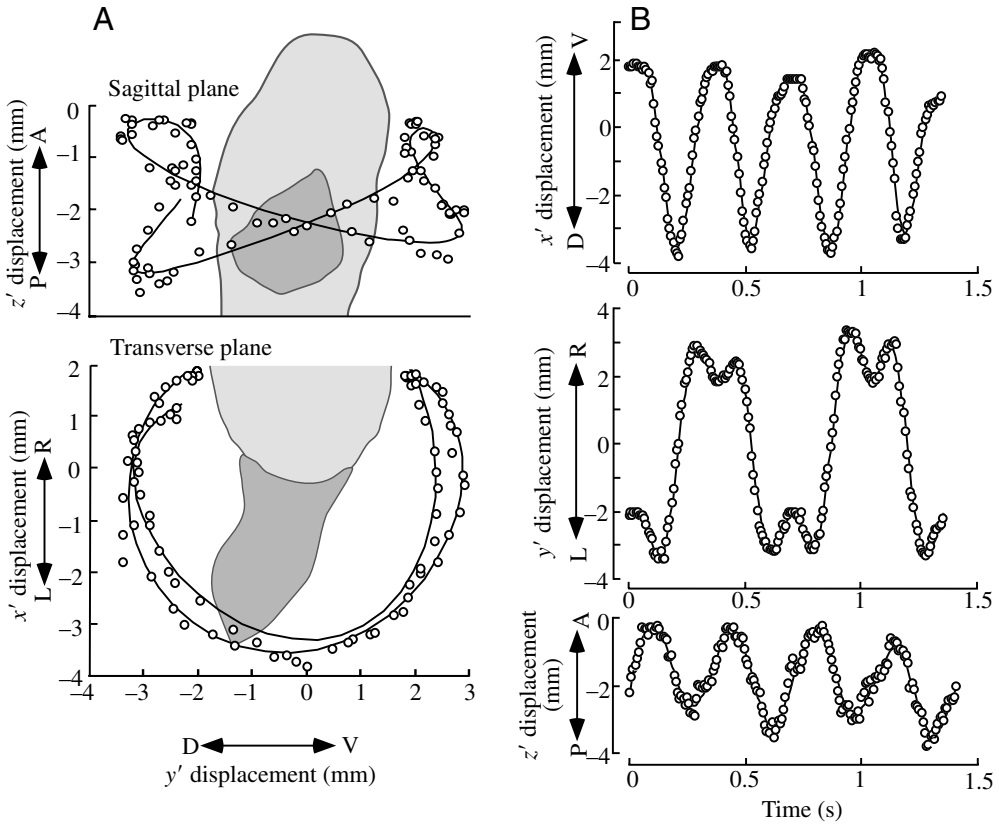

Fig. 2. (A) Right lateral and dorsal views of wingtip displacement relative to the wing base for *Clione antarctica* (individual no. 1) swimming at 0.3°C. (B) Wingtip position *vs* time for two wingbeat cycles. Circles represent the position of digitized data points, and plotted lines are spline functions fitted to time series data. P, posterior; A, anterior; D, dorsal; V, ventral; R, right; L, left.

mean wingtip velocity) ranged from 0.06 to 0.18, indicating that unsteady effects may be important, particularly in the larger animals (see Table 1).

The stroke plane angle, β, is largely orthogonal to the longitudinal body axis (β=1.98±1.65°), but the power stroke plane angle, β_{ps}, ranges from 18.5° to 31.7°, with a mean of 24.8±1.7°. At low velocities, β_{ps} is fairly shallow, but increases at higher translational velocities of the body (Fig. 4).

At midstroke, the wing surface is oriented at 46.0±4.3° relative to the body y'-axis. In some sequences, this angle is fixed early in the power phase of the upstroke, whereas in others, rotation about the longitudinal wing axis is more continuous. The mean value of α at midstroke was 71.4±2.2° and ranged from 62.6° to 80.3°. Because α depends on β_{ps}, steeper angles of attack were also associated with higher body translational velocities (see Fig. 4).

Body kinematics

C. antarctica ascends at absolute velocities ranging from 1 to 7 mm s^{-1}, corresponding to non-dimensional velocities from 0.35 to 1.87, respectively, and to *Re* between 6 and 49, respectively (see Table 1). The mean angle of ascent, ξ, is largely coincident with the sum of mean body angle $\overline{\chi}$ and β. However, the trajectory of an ascending pteropod is punctuated by cyclic oscillations due to large asymmetrical forces produced by the wings during each half-stroke. Body motions follow a saw-toothed path, and at the end of each half-stroke the body slows to a halt before the subsequent half-stroke is initiated (Fig. 5). The mean angle of ascent during the power stroke was 64.7±2.2°, and increased with non-dimensional body velocity (see Fig. 4). This angle of ascent was largely perpendicular to the wing surface. The three individuals with Re_{body}<25, exhibited downwards body motion (i.e. negative translational velocities) during the recovery phase. Of the other seven individuals, only individual no. 10, with an unusually long recovery stroke, exhibited net downwards motion.

Maximum positive fore–aft accelerations occurred at the beginning of the power phase of each half-stroke (at $\hat{t}$=0.05 and $\hat{t}$=0.52 for the up- and downstroke, respectively; Figs 6, 7). Wingtip velocity and thus translational hydrodynamic forces peak after body has reached its maximum vertical acceleration (Fig. 7). Peak fore–aft acceleration of the wingtip, however, immediately precedes these accelerational maxima of the body.

We calculated dorsoventral deviations of the body from the mean trajectory of the pteropod during a wingbeat. On average, the body reached a maximum deviation of 16–17% of the wing length. The timing of maximum deviations was nearly the same for the upstroke and the downstroke, with maximum displacement in the dorsal direction occurring at $\hat{t}$=0.47, and in the ventral direction at $\hat{t}$=0.98. The body exhibited zero displacement from the mean trajectory at $\hat{t}$=0.22 and $\hat{t}$=0.74. Ellington (1984a) used quasi-steady aerodynamic assumptions to show that translational oscillations in body position should be proportional to R^4 m^{-1} in hovering animals. (Note that this analysis assumed no restorative torques associated with drag and acceleration reactions on the body). For the *C. antarctica* sequences analyzed here, the magnitude of dorsoventral

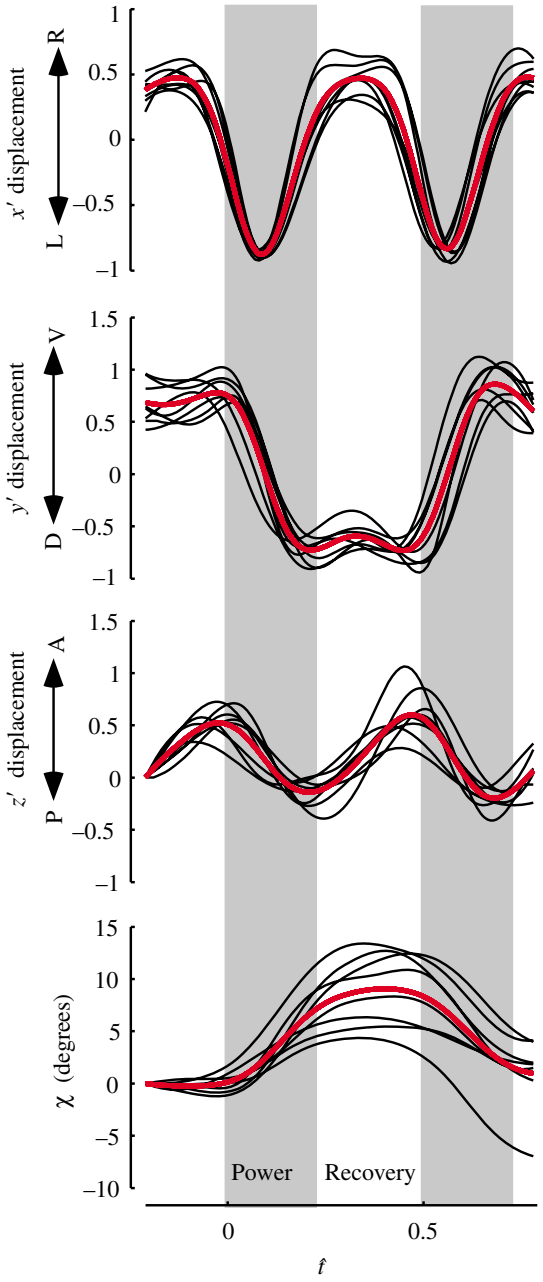

Fig. 3. Relative wingtip position and relative body angle during a complete wingbeat cycle for *Clione antarctica*. Thin lines are interpolated points from a spline function fitted to digitized kinematic data from individual sequences. Thick red lines represent the mean value for all kinematic sequences. P, posterior; A, anterior; D, dorsal; V, ventral; R, right; L, left.

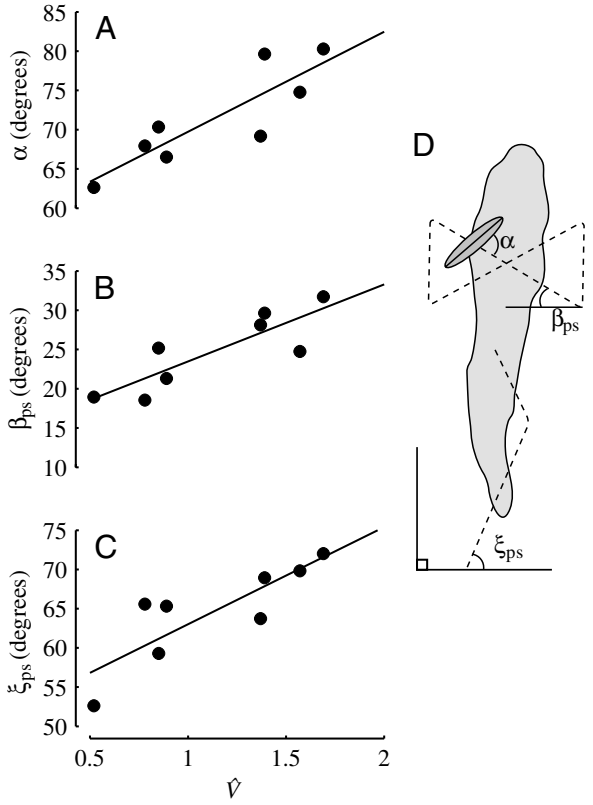

Fig. 4. Kinematic parameters as a function of non-dimensional body velocity in *Clione antarctica*. (A) Angle of attack (α) increases with non-dimensional velocity (r^2=0.741, $F_{1,6}$=17.155, P=0.0061); (B) stroke plane angle during the power phase (β_{ps}) increases with non-dimensional velocity (r^2=0.725, $F_{1,6}$=15.780, P=0.0073); (C) angle of ascent during the power phase (ξ_{ps}) increases with non-dimensional velocity (r^2=0.701, $F_{1,6}$=14.099, P=0.0095); (D) kinematic definitions of angle of attack, stroke plane angle during the power phase, and ascent angle.

deviations showed no significant change with body mass, wing length, or the quantity R^4 m^{-1}.

In addition to inducing oscillations of the center of mass, forces produced by the flapping wings also act on the moment arm between the wing bases and the center of body mass, causing the body angle to oscillate during a wingbeat. During a half-stroke, *Clione* oscillates through an average angle of 11.0±1.0° (Fig. 3). These oscillations exhibit a significant decrease in amplitude with body mass (r^2=0.8, P=0.0005). On average, maximum and minimum values of χ occur at $\hat{t}$=0.44 and $\hat{t}$=0.9, respectively, during the recovery phase at the end of each half-stroke (Fig. 3). Maximum angular accelerations occur at the beginning of the power phase of each half-stroke (i.e. $\hat{t}$=0.07 for the upstroke, and $\hat{t}$=0.55 for the downstroke), and maximum decelerations occur at the beginning of each recovery phase ($\hat{t}$=0.26 for the upstroke, and $\hat{t}$=0.75 for the downstroke; Fig. 8). Dorsoventral accelerations of the wingtip precede these body accelerations, whereas wingtip velocities peak after maximum body accelerations (Fig. 9).

Discussion

Hydrodynamic interpretation

In comparison to other aquatic and aerial flyers, the mean *AR* of *Clione antarctica*, at 2.5, is relatively low. Traditionally, low *AR* was thought to be indicative of a decreased lift-to-drag ratio, because the deleterious influence of tip vortices on airfoil lift performance becomes relatively greater (Vogel, 1994).

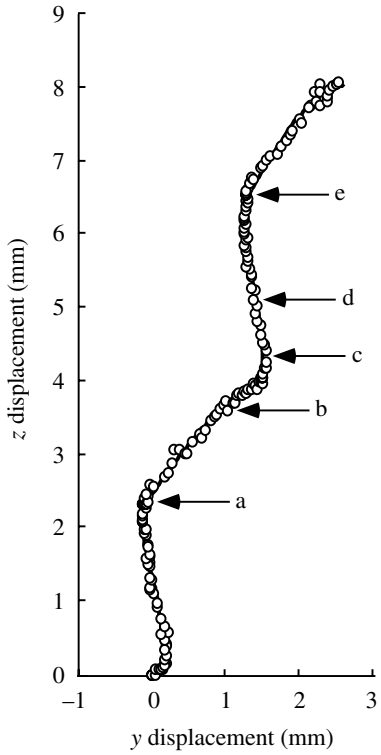

Fig. 5. Lateral projection of the geometric center of area of a *Clione antarctica* (individual no. 1) in vertical ascent during two complete wingbeat cycles. Arrows denote: a, the beginning of the power phase of the upstroke; b, recovery phase of the upstroke; c, power phase of downstroke; d, recovery phase of the downstroke; and e, the end of the stroke cycle.

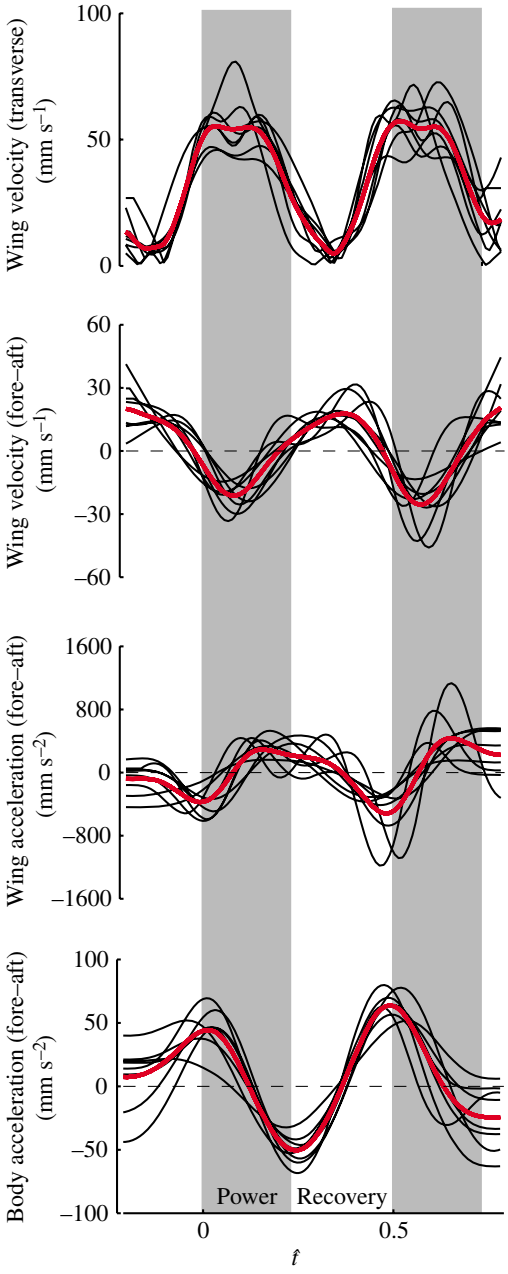

Fig. 6. Fore–aft acceleration of the body in relation to three wingtip variables: fore–aft velocity, fore–aft acceleration, and transverse (lateral and dorsoventral components) velocity. Thin lines are estimated from the second derivative of a spline function fitted to the digitized kinematics from individual sequences. Thick lines represent mean values averaged across all eight sequences.

Usherwood and Ellington (2002) showed for high *Re,* however, that variation in *AR* from 4.5 to 15.8 had little influence on the lift performance of revolving model hawkmoth wings at angles of attack less than 50°. However, at the higher angles of attack more representative of those used by pteropods, low *AR* wings did indeed suffer diminished lift-to-drag ratios. Although patterns of fluid flow may differ substantially over the range of *Re* being compared (Birch et al., 2004), pteropods may be ill-equipped to propel themselves *via* lift forces on the basis of wing morphology alone. Effects of rotational circulation may also be small given the reduced wing rotational velocities associated with very slow half-stroke transitions at flapping frequencies of only several Hz.

Kinematics of the wingtip and body provide further support for the assertion that *C. antarctica* is using its wing primarily as a paddle and not as an hydrofoil. First, the angles of attack were high, ranging from 60° in the slowest swimmers to 80° in the fastest ones. At *Re* of 160, the lift coefficient of a model insect wing declines substantially as the angle of attack increases from 60° to 80°, and the lift-to-drag ratio is maximal at much lower angles of attack, namely between 20° and 40° (Sane and Dickinson, 2001). Although circulation certainly develops around the flapping pteropod wing, lift produced during wing translation is unlikely to be an important component in the overall force balance during flapping ascent. Indeed, the stroke plane angle of the power phase as well as the wing's angle of attack increase with swimming velocity, which would serve to orient drag forces more vertically and any potential lift forces more dorsoventrally. In addition, the fact that the wing surface is nearly perpendicular to the pteropod's ascent trajectory during the power phase provides

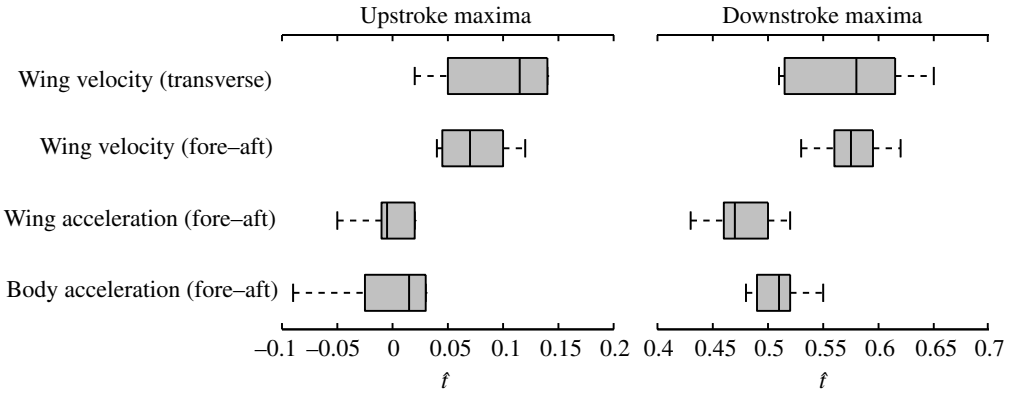

Fig. 7. Timing of kinematic events in relation to fore–aft accelerations of the body based on data from eight *Clione* individuals as shown in Fig. 6. Inflection points not unambiguously identified were excluded from the analysis. The central line indicates the median value, the grey box delimits the upper and lower quartiles, and whiskers indicate the range of the remaining data.

further support for the inference of drag-based locomotion. By ruling out lift as an important propulsive mechanism for *C. antarctica*, these results buttress a general conclusion that lift-based flapping is ineffective at *Re*<100 (Bennett, 1972; Daniel and Webb, 1987; Horridge, 1956; Webb and Weihs, 1986).

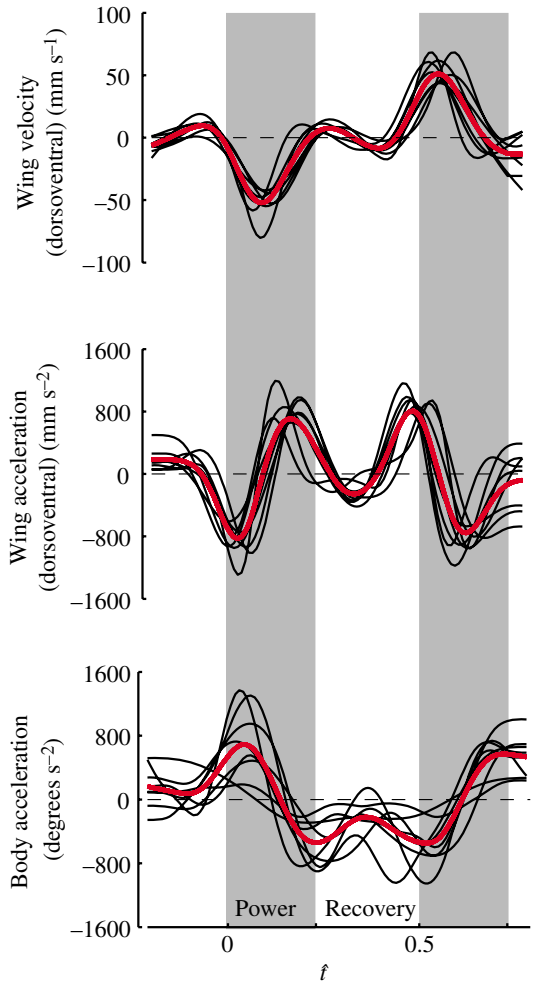

Fig. 8. Dorsoventral components of wingtip velocity and acceleration, and rotational acceleration of the body for ascending *Clione antarctica*. Thin lines are estimated from the first derivative of a spline function fitted to digitized kinematic data from individual sequences. Thick red lines represent the mean values averaged across all eight sequences.

The tiny wasp *Encarsia formosa* oscillates its wings at an *Re* of 17 (Weis-Fogh, 1973), but it is unclear whether it and other minute flying insects employ lift-based locomotion or are simply rowing through the air (Bennett, 1972; Horridge, 1956; Thompson, 1942).

The potential role of unconventional mechanisms of force generation in the rowing locomotion of *C. antarctica*, and of other organisms operating at *Re* between 10 and 100, merits further investigation. In *C. antarctica*, large forces must be produced at stroke initiation because of the rapid accelerations estimated for the center of body mass. For a model insect wing, Sane and Dickinson (2001, 2002) demonstrated that force transients at stroke initiation are primarily due to wake recapture, although smaller peaks during impulsive starts at stroke transitions are caused by the acceleration reaction as they precede vortex formation (Birch and Dickinson, 2003). Overall, forces produced by the acceleration reaction are approximately equal in magnitude to those produced *via* wing rotation, but are on average small in comparison with translational aerodynamic forces (Sane and Dickinson, 2002). The acceleration reaction clearly plays a role in propulsion at much higher *Re* (>1000), as exemplified by such diverse locomotor modes as the rowing of dytiscid beetles (Nachtigall, 1980), frogs (Gal and Blake, 1988a,b), the jet propulsion of medusae (Daniel, 1983), and the tail-flick of carridean shrimp (Daniel and Meyhöfer, 1989). However, by combining kinematic data, force measurements and blade-element modeling, McHenry et al. (2003) demonstrated that the acceleration reaction is negligible in the undulatory swimming of ascidian larvae (1<*Re*<100). Similarly, Williams (1994a,b) used kinematic results, physical models and theoretical analysis to discount the importance of the acceleration reaction in rowing *Artemia* (for which 1<*Re*<10). Downwards acceleration of the mass of the muscular wing itself may also contribute to vertical force production in pteropods. Body acceleration is more tightly phase-coupled to wing acceleration than to peak wing fore–aft velocity (see Fig. 6), a finding consistent with accelerational effects of either the wing mass or the wing added mass. To conclusively evaluate the relative importance of wing inertia, rotational circulation, the acceleration reaction and wake recapture in rowing locomotion at these *Re*, we suggest similar integrative approaches in future

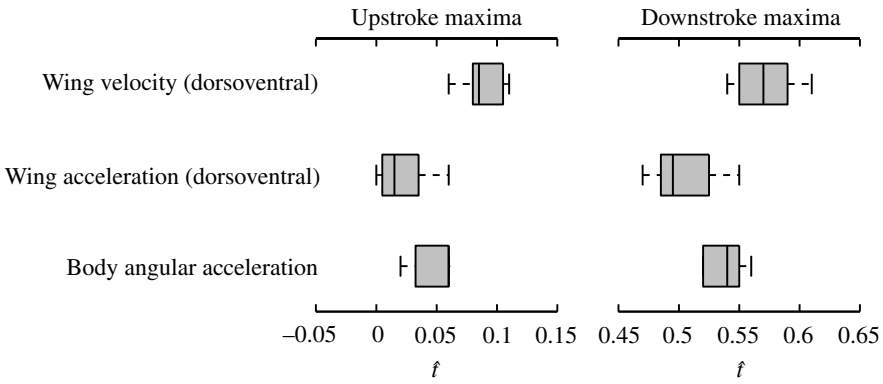

Fig. 9. Timing of kinematic events in relation to angular accelerations of the body based on data from the eight *Clione* individuals shown in Fig. 8. Inflection points not unambiguously identified were excluded from analysis. The central line indicates the median value, the grey box delimits the upper and lower quartiles, and whiskers indicate the range of the remaining data.

studies of pteropod locomotion, in particular quantification of flows.

Rowing with flexible paddles

Wing–body interactions and wing flexibility may also confound direct comparison of pteropod hydrodynamics with those derived empirically from the mechanical flapping of rigid model wings. Whereas pterygote insects possess wing veins and volant vertebrates use bones to support their wings, pteropod wings are a modification of the generalized molluscan foot and lack any rigid support. As pteropods row, they not only change the position of the wingtip in space but also alter the shape of the wing itself. At mid-stroke, the wing is nearly straight, but at the end of each half-stroke it is adpressed to the body, forming a tight arc. Such flexibility may allow the wing to remain within the boundary layer surrounding the body during the recovery phase of each half-stroke. One of the major problems with drag-based propulsion at low *Re* is that, during the recovery stroke, the drag on an appendage oriented parallel to flow may be only slightly less than that when perpendicular to flow (Walker, 2002). Pteropods may partially mitigate this problem by removing their appendages from the free-stream velocity during recovery. During the beginning and end of each half-stroke, *C. antarctica* may also utilize 'peel-like behavior' reminiscent of 'clap and fling' and squeeze mechanisms previously described in other taxa (Daniel and Meyhöfer, 1989; Ellington, 1984b; Weis-Fogh, 1973), and proposed for pteropods (Satterlie et al., 1985). Such body interactions are explicitly addressed elsewhere in a hydrodynamic model of pteropod swimming (Childress and Dudley, 2004). Overall, the distinctive kinematic features of the pteropod wingbeat exploit largely drag-based force production during the power phase of each half-stroke, together with a recovery phase enabled by low aspect ratio and flexible wings pressed close to the body. This mode of locomotion therefore uniquely combines flapping and rowing motions, and is distinct from other drag-based stroke regimes that rely on asymmetry between half-strokes to effect recovery to the starting position of the stroke.

The hydrodynamic implications of curvature of pteropod at midstroke are unclear. The wings of insects, bats and numerous other flying and swimming animals deform under inertial loads (Ennos, 1988, 1989; Swartz et al., 1996; Wootton, 1981), and fluid-dynamic loading is particularly important for wings of aquatic swimmers (Combes and Daniel, 2003; Daniel and Combes, 2002). Wing deformation in some flies may advantageously alter lift production (Ennos, 1988). In pteropods, positive camber likely derives from internal hydrostatic pressure and also from contraction of radial and concentric muscle fibers in the wing. Active wing flexion can contribute significantly to force production and enhanced efficiency in flapping flight, but this phenomenon may be restricted to higher *Re* (Combes and Daniel, 2001). Rotation of the pteropod wing at the ends of half-strokes, albeit as constrained anatomically by the relatively large wing base, must also contribute to the patterns of deformation seen during the wingbeat.

Neuromuscular control of swimming speed

The ability to alter swimming speed is critical during predator–prey interactions during which changes in translational and rotational velocities are essential. *Clione limacina*, a pteropod found in the temperate zone, exhibits two types of escape behaviors: a withdrawal response and an escape swimming response (Norekian and Satterlie, 2001). This pteropod species normally exhibits a slow swimming behavior characterized by a flapping frequency of 1–2 Hz; upwards propulsion barely exceeds negative buoyancy (Satterlie et al., 1990). When disturbed, however, these pteropods increase flapping frequency substantially to a maximum of 10 Hz, and ascent velocity approaches 100 mm s^{-1}, approximately seven body lengths per second. This response is mediated by the release of serotonin, which increases the cycle frequency of the central pattern generator (Satterlie and Norekian, 1996). By contrast, *C. antarctica* failed to show an escape swimming response during our experimental trials with over 400 individuals, and always showed a withdrawal response in reaction to even the slightest disturbance. This withdrawal response involved apparent inhibition of the swimming motoneurons, retraction of the wings, conglobation and sinking. In *C. limacina*, such withdrawal behavior occurs only when the animal is confronted with the most extreme stimuli (Norekian and Satterlie, 1996). We suspect that the increased expression of the withdrawal response in *C. antarctica* is due, at least in part, to the apparent inability to substantially increase flapping frequency necessary for an escape swimming response.

Although *C. antarctica* does not exhibit a two-gear swimming

behavior, ascent velocity is positively correlated with flapping frequency even within the small range of 1–2 Hz (R.D., B.J.B. and J.A.G., unpublished data). In pteropods, stroke amplitude is near maximal during ascent swimming at all velocities, being geometrically constrained by the presence of the body. Our present results suggest that additional aspects of wingbeat kinematics may be important in the control of swimming speed. In particular, changes in the inclination angle of the power phase of each half-stroke will alter the effective angle of attack of the wing: steeper power phases are associated with reduced body oscillations and a greater ascent velocity. This situation is analogous to that of in flying insects, for which increased stroke plane angles are strongly associated with increasing forward velocity (see Dudley, 2000). This shift in stroke plane angle tilts the net aerodynamic force vector forwards, yielding additional thrust but also maintaining vertical force production. It is likely that individual pteropods similarly modulate swimming speed *via* such a mechanism, although a challenge for future studies will be to determine how the amplitude and timing of muscle activation within the wingbeat cycle contributes to the complex geometry of the wingtip path, and ultimately to the production of variable hydrodynamic forces at different locomotor speeds.

List of symbols

AR	aspect ratio
$\bar{c}$	mean wing chord
J	advance ratio
L	body length
M_b	body mass
n	wingbeat frequency
R	wing length
Re_b	Reynolds number of the body
Re_w	Reynolds number of the wing
S	surface area of the wing pair
$\hat{t}$	non-dimensional time
$\hat{V}$	non-dimensional velocity
α	angle of attack
β	mean stroke plane angle over the entire stroke
β_{ps}	stroke angle of the power phase in each half-stroke
χ	body angle
$\bar{\chi}$	mean body angle
ξ	mean angle of ascent of the body during a half-stroke
ξ_{ps}	angle of ascent of the body during the power phase of a half-stroke

We thank the staff at McMurdo station for providing outstanding logistical support during the course of this project. B. Seibel, J. Rosenthal, and F. Bezanilla taught us about the muscular and neural systems involved in *Clione* locomotion. We also thank S. Combes, J. Strother, S. Sane, and two anonymous reviewers for patient and constructive criticism regarding our fluid dynamic inferences, although any interpretational errors are strictly our own. This research was funded by NSF OPP-9980360 to R.D. and a NSF Graduate Research Fellowship to B.B.

References

Bellwood, D. R. and Wainwright, P. C. (2001). Locomotion in labrid fishes: Implications for habitat use and cross-shelf biogeography on the Great Barrier Reef. *Coral Reefs* **20**, 139-150.

Bennett, L. (1972). Effectiveness and flight of small insects. *Ann. Entomol. Soc. Am.* **66**, 1187-1190.

Birch, J. M. and Dickinson, M. H. (2003). The influence of wing–wake interactions on the production of aerodynamic forces in flapping flight. *J. Exp. Biol.* **206**, 2257-2272.

Birch, J. M., Dickson, W. B. and Dickinson, M. H. (2004). Force production and flow structure of the leading edge vortex on flapping wings at high and low Reynolds numbers. *J. Exp. Biol.* **207**, 1063-1072.

Childress, S. and Dudley, R. (2004). Transition from ciliary to flapping mode in a swimming mollusc: flapping flight as a bifurcation in Re_ω. *J. Fluid Mech.* **498**, 257-288.

Combes, S. A. and Daniel, T. L. (2001). Shape, flapping and flexion: wing and fin design for forward flight. *J. Exp. Biol.* **204**, 2073-2085.

Combes, S. A. and Daniel, T. L. (2003). Into thin air: contributions of aerodynamic and inertial-elastic forces to wing bending in the hawkmoth *Manduca sexta*. *J. Exp. Biol.* **206**, 2999-3006.

Daniel, T. L. (1983). Mechanics and energetics of medusan jet propulsion. *Can. J. Zool.* **61**, 1406-1420.

Daniel, T. L. (1984). Unsteady aspects of aquatic locomotion. *Am. Zool.* **24**, 121-134.

Daniel, T. L. and Combes, S. A. (2002). Flexible wings and fins: bending by inertial or fluid-dynamic forces. *Integr. Comp. Biol.* **42**, 1044-1049.

Daniel, T. L. and Meyhöfer, E. (1989). Size limits in escape locomotion of carridean shrimp. *J. Exp. Biol.* **143**, 245-266.

Daniel, T. L. and Webb, P. W. (1987). Physical determinants of locomotion. In *Comparative Physiology: Life In Water and On Land* (ed. P. Dejours, L. Bolis, C. R. Taylor and E. R. Weibel), pp. 343-369. New York: Liviana Press.

Daniel, T. L., Jordan, C. and Grunbaum, D. (1992). Hydromechanics of swimming. In *Mechanics of Animal Locomotion* (ed. R. M. Alexander), pp. 17-49. Berlin: Springer-Verlag.

Dudley, R. (2000). *The Biomechanics of Insect Flight: Form, Function, and Evolution.* Princeton: Princeton University Press.

Ellington, C. P. (1984a). The aerodynamics of hovering insect flight. III. Kinematics. *Proc. R. Soc. Lond. B* **305**, 41-78.

Ellington, C. P. (1984b). The aerodynamics of hovering insect flight. IV. Aerodynamic mechanisms. *Proc. R. Soc. Lond. B* **305**, 79-113.

Ellington, C. P. (1984c). The aerodynamics of hovering insect flight. V. A vortex theory. *Proc. R. Soc. Lond. B* **305**, 115-144.

Ennos, R. (1988). The importance of torsion in the design of insect wings. *J. Exp. Biol.* **140**, 137-160.

Ennos, R. (1989). Inertial and aerodynamic torques on the wings of Diptera in flight. *J. Exp. Biol.* **142**, 87-95.

Fish, F. E. (1996). Transitions from drag-based to lift-based propulsion in mammalian swimming. *Am. Zool.* **36**, 628-641.

Fuiman, L. A. and Batty, R. S. (1997). What a drag it is getting cold: partitioning the physical and physiological effects of temperature on fish swimming. *J. Exp. Biol.* **200**, 1745-1755.

Gal, J. M. and Blake, R. W. (1988a). Biomechanics of frog swimming I. Estimation of the propulsive force generated by *Hymenochirus boettgeri*. *J. Exp. Biol.* **138**, 399-411.

Gal, J. M. and Blake, R. W. (1988b). Biomechanics of frog swimming II. Mechanics of the limb-beat cycle in *Hymenochirus boettgeri*. *J. Exp. Biol.* **138**, 413-429.

Horridge, G. A. (1956). The flight of very small insects. *Nature* **178**, 1334-1335.

McHenry, M. J., Azizi, E. and Strother, J. A. (2003). The hydrodynamics of locomotion at intermediate Reynolds numbers: undulatory swimming in ascidian larvae (*Botrylloides* sp.). *J. Exp. Biol.* **206**, 327-343.

Morton, J. E. (1954). The biology of *Limacina retroversa*. *J. Mar. Biol. Assn. UK* **33**, 297-312.

Morton, J. E. (1958). Observations on the gymnostomatous pteropod *Clione limacina* (Phipps). *J. Mar. Biol. Assoc. UK* **37**, 287-297.

Nachtigall, W. (1980). Mechanics of swimming water-beetles. In *Aspects of Animal Movement* (ed. H. Y. Elder and E. R. Trueman), pp. 107-124. Cambridge: Cambridge University Press.

Norekian, T. and Satterlie, R. A. (1996). Whole-body withdrawal system and its involvement in the behavioral hierarchy of the mollusc *Clione limacina*. *J. Neurophysiol.* **75**, 529-537.

Norekian, T. and Satterlie, R. A. (2001). Serotonergic neural system not only

activates swimming but also inhibits competing neural centers in a pteropod mollusc. *Am. Zool.* **41**, 993-1000.
Podolsky, R. D. and Emlet, R. B. (1993). Separating the effects of temperature and viscosity on swimming and water movement by sand dollar larvae (*Dendraster excentricus*). *J. Exp. Biol.* **176**, 207-221.
Sane, S. P. (2003). The aerodynamics of insect flight. *J. Exp. Biol.* **206**, 4191-4208.
Sane, S. P. and Dickinson, M. H. (2001). The control of flight force by a flapping wing: lift and drag production. *J. Exp. Biol.* **204**, 2607-2626.
Sane, S. P. and Dickinson, M. H. (2002). The aerodynamic effects of wing rotation and a revised quasi-steady model of flapping flight. *J. Exp. Biol.* **205**, 1087-1096.
Satterlie, R. and Norekian, T. (1996). Serotonergic modulation of swimming speed in the pteropod mollusc *Clione limacina*. III. Cerebral neurons. *J. Exp. Biol.* **198**, 917-930.
Satterlie, R. A., Labarbera, M. and Spence, A. N. (1985). Swimming in the pteropod mollusc, *Clione limacina.* I. Behavior and morphology. *J. Exp. Biol.* **116**, 189-204.
Satterlie, R. A., Goslow, G. E. and Reyes, A. (1990). Two types of striated muscle suggest two-geared swimming in the pteropod mollusc, *Clione limacina*. *J. Exp. Zool.* **255**, 131-140.
Swartz, S. M., Groves, M. S., Kim, H. D. and Walsh, W. R. (1996). Mechanical properties of bat wing membrane skin. *J. Zool.* **239**, 357-378.
Thompson, D. A. W. (1942). *On Growth and Form*. Cambridge: Cambridge University Press.
Usherwood, J. R. and Ellington, C. P. (2002). The aerodynamics of revolving wings. II. Propeller force coefficients from mayfly to quail. *J. Exp. Biol.* **205**, 1565-1576.
Vogel, S. (1994). *Life in Moving Fluids.* Princeton: Princeton University Press.
Walker, J. (2002). Functional morphology and virtual models: physical constraints on the design of oscillating wings, fins, legs, and feet at intermediate Reynolds numbers. *Integr. Comp. Biol.* **42**, 232-242.
Walker, J. A. (1998). Estimating velocities and accelerations of animal locomotion: a simulation experiment comparing numerical differentiation algorithms. *J. Exp. Biol.* **201**, 981-995.
Walker, J. A. and Westneat, M. N. (1997). Labriform propulsion in fish kinematics of flapping aquatic flight in the bird wrasse *Gomphosus varius* (Labridae). *J. Exp. Biol.* **200**, 1549-1569.
Walker, J. A. and Westneat, M. W. (2000). Mechanical performance of aquatic rowing and flapping. *Proc. R. Soc. Lond. B* **267**, 1875-1881.
Webb, P. W. and Weihs, D. (1986). Functional locomotor morphology of early life history stages of fishes. *Trans. Am. Fish. Soc.* **115**, 115-127.
Weis-Fogh, T. (1973). Quick estimates of flight fitness in hovering animals, including novel mechanisms for lift production. *J. Exp. Biol.* **59**, 169-230.
Williams, T. A. (1994a). Locomotion in developing *Artemia* larvae: mechanical analysis of antennal propulsors based on large-scale physical models. *Biol. Bull.* **187**, 156-163.
Williams, T. A. (1994b). A model of rowing propulsion and the ontogeny of locomotion in *Artemia* larvae. *Biol. Bull.* **187**, 164-173.
Wootton, R. J. (1981). Support and deformability in insect wings. *J. Zool.* **193**, 447-468.